On-Chip Generation and Collectively Coherent Control of the Superposition of the Whole Family of Dicke States

Leizhen Chen,[1] Liangliang Lu,[1,2] Lijun Xia,[1] Yanqing Lu,[1] Shining Zhu,[1] and Xiao-song Ma[1,3,4,*]
[1]National Laboratory of Solid-state Microstructures, School of Physics, College of Engineering and Applied Sciences, Collaborative Innovation Center of Advanced Microstructures, Nanjing University, Nanjing 210093, China
[2]Key Laboratory of Optoelectronic Technology of Jiangsu Province, School of Physical Science and Technology, Nanjing Normal University, Nanjing 210023, China
[3]Synergetic Innovation Center of Quantum Information and Quantum Physics, University of Science and Technology of China, Hefei, Anhui 230026, China
[4]Hefei National Laboratory, Hefei 230088, China

(Received 23 September 2022; revised 2 January 2023; accepted 28 April 2023; published 30 May 2023)

Integrated quantum photonics has recently emerged as a powerful platform for generating, manipulating, and detecting entangled photons. Multipartite entangled states lie at the heart of the quantum physics and are the key enabling resources for scalable quantum information processing. Dicke state is an important class of genuinely entangled state, which has been systematically studied in the light-matter interactions, quantum state engineering, and quantum metrology. Here, by using a silicon photonic chip, we report the generation and collectively coherent control of the entire family of four-photon Dicke states, i.e., with arbitrary excitations. We generate four entangled photons from two microresonators and coherently control them in a linear-optic quantum circuit, in which the nonlinear and linear processing are achieved in a chip-scale device. The generated photons are in telecom band, which lays the groundwork for large-scale photonic quantum technologies for multiparty networking and metrology.

DOI: 10.1103/PhysRevLett.130.223601

Introduction.—Multipartite quantum states with rich structures are extensively investigated [1] and are regarded as core components for implementing quantum information processing tasks. For example, particular multipartite entangled states known as cluster or graph states are universal resources for quantum computation [2–5]. Other states can achieve sub-shot-noise sensitivity in phase estimation, attracting increasing interest in the field of quantum enhanced metrology [6–8]. These have triggered high demand for generating and coherent controlling multipartite entanglement. Dicke state [9] is an important state due to its entanglement being robust against the loss of particles and attractive for practical applications such as multiparty quantum networking [10,11] and quantum metrology [12]. The Dicke states can also serve as a versatile resource for preparing states of different entanglement classes with lower particle numbers through the projective measurements on individual qubits [10]. Note that generalized parity measurements and ancilla qudits can be employed to prepare Dicke states [13].

Generally, an N-qubit Dicke state with m excitations is defined as the equal superposition of all basis states and written in the following form:

$$|D_N^m\rangle = \frac{1}{\sqrt{C_N^m}} \sum_m P_m |0^{N-m}1^m\rangle, \tag{1}$$

where $\sum_m P_m(\cdots)$ represents the sum over all possible permutations for m excitations among the N particles. In qubit language, $|0^{N-m}1^m\rangle$ stands for m qubits in $|1\rangle$ state, and $N-m$ qubits in $|0\rangle$ state.

Dicke states have been realized in a variety of physical systems, including photons [10–12,14], trapped ions [15], cold atoms [16–18], and superconducting systems [19–21]. The past research efforts mainly focused on one or two types of Dicke states, such as those with one or $(N/2)$ excitations distributed within N particles. In particular, photonic systems emerge as a desirable quantum platform owing to the features of weak coupling to the surroundings, individual addressability, and high-fidelity qubit operation, opening up ways to systematically study multipartite entanglement. So far, all photonic Dicke states with specific excitations are generated from bulk optical setups with static generation configurations. The photons generated in these experiments are around 800 nm, which is unsuitable for long-distance transmission because of the signal attenuation in fibers. Photons at telecom wavelength are more applicable to long-distance communications due to the low loss in fibers and the use of standard high-performance fiber components [22]. Integrated quantum photonics on silicon, compatible with complementary metal-oxide-semiconductor fabrication, offer intrinsic high optical nonlinearity, dense integration, and excellent phase stability and can therefore provide a natural solution for photonic

 © 2023 American Physical Society

quantum technology. Hundreds of optical components have been integrated onto a single silicon chip, realizing the complex photonic circuits needed to generate and manipulate photon states and achieve large-scale quantum information processing [23,24]. Recently, the on-chip generation of two-photon Bell state [25], near-ideal two-photon source [26], four-photon Greenberger-Horne-Zeilinger (GHZ) state [27], and cluster state [28] have been realized with silicon chips. Here, we use integrated photonics to generate the coherent superposition of the entire family of the four-photon Dicke states. Moreover, we harness the advantage of integrated photonics to collectively control all four photons and demonstrate the coherence of various Dicke states. Specifically, we create the path-encoded four-photon Dicke states by using two identical dual Mach-Zehnder interferometer microring (DMZI-ring) photon-pair sources [29–32]. Field enhancement and independent tuning capabilities of the coupling coefficients of pump, signal, and idler photons allow the generation of single photons with high indistinguishability and brightness without using passive filtering. High-fidelity multiphoton operation is realized by linear optics network. All the nonlinear and linear quantum devices are monolithically integrated in silicon. We experimentally observe and coherently control for the first time, to our knowledge, the superposition of the entire family of four-photon Dicke states in the telecom band, which can easily interface with fiber quantum network, implying the flexibility and multiformity of our device.

Experimental setup.—The experimental generation of the multiphoton Dicke state works based on the scheme shown in Fig. 1. Let us start with a two-photon source, made by S1 and S2 [Fig. 1(a)]. We use the following path encoding: S1 could generate two photons in path 0; S2 could generate two photons in path 1. Both sources are coherently pumped by a single laser. After photons in path 1 experience a relative phase ϕ to those in path 0, a linear optical network consisting of beam splitters and waveguides combines and splits the path modes 0 and 1. Detecting both photons from the sources, we obtain a two-photon entangled state with the superposition of two Bell states:

$$|\Psi_2(\phi)\rangle = \cos\phi|\Psi^+\rangle - \sin\phi|\Phi^-\rangle, \tag{2}$$

where $|\Psi^+\rangle = 1/\sqrt{2}(|01\rangle + |10\rangle)$ and $|\Phi^-\rangle = 1/\sqrt{2}(|00\rangle - |11\rangle)$. Note that $|01\rangle$ stands for $|0\rangle_A \otimes |1\rangle_B$, in which $|0_A\rangle$ ($|1_A\rangle$) denotes logical value 0 (1) for the dual-rail encoded photonic qubit A. In this process, we employ the time-reversed Hong-Ou-Mandel (RHOM) interference between identical photon pairs [25,33,34], and Bell-state projection. In this way, the two-photon entangled state and its coherent superposition are created and are controlled via phase ϕ.

We further consider the probability of two pairs of photons generated at the same time [Fig. 1(b)]. A four-photon entangled state is obtained when four detectors in each of the four modes respond simultaneously [10].

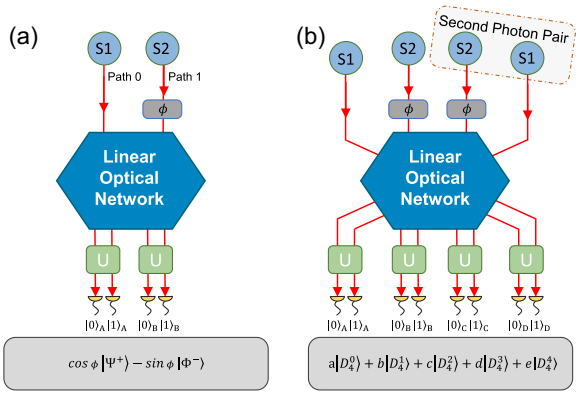

FIG. 1. Concept of multiphoton entanglement creation and control. (a) Tunable entangled photon pair generation. A qubit-pair module, consisting of two photon-pair sources (S1 and S2), is coherently pumped. The generated photons are then controlled and combined with beam splitters. The generated quantum state is an entangled two-qubit state after interference on the network, as shown in Eq. (2). This state is then analyzed by universal qubit analyzers (Us) for implementing arbitrary local projective measurements. (b) Tunable entangled four-photon generation. The sources generate two pairs of photons simultaneously. The detections in four detectors result in the generation of the superposition of the whole family of four-photon Dicke states, as shown in Eq. (3). For both the two-photon state and the four-photon state, the phase shift ϕ can control all photons coherently and adjust the weights of the respective states.

After the linear optical network, we obtain a four-qubit entangled state with the superposition of the whole family of four-photon Dicke states:

$$\begin{aligned}|\Psi_4(\phi)\rangle = \frac{1}{2\sqrt{6}}\Big\{&3\sin^2\phi|D_4^0\rangle - 6\sin\phi\cos\phi|D_4^1\rangle \\ &+ \sqrt{6}(3\cos^2\phi - 1)|D_4^2\rangle + 6\sin\phi\cos\phi|D_4^3\rangle \\ &+ 3\sin^2\phi|D_4^4\rangle\Big\}.\end{aligned} \tag{3}$$

By adjusting the relative phase ϕ, we create various superpositions of all five four-photon Dicke states. Note that the equally weighted superposition of $|D_4^0\rangle$ and $|D_4^4\rangle$ corresponds to a GHZ state, and $|D_4^1\rangle$ and $|D_4^3\rangle$ are W states [35], respectively. Postselection of one photon per dual-rail qubit plays an important role in this device, and indeed is the source of the measured entanglement. The theoretical postselection efficiency of the four-photon state is 3/32. The details on the evolution and the postselection for the two- and four-photon states, and the scalability of this multipartite entangled state with higher photon numbers can be found in the Supplemental Material [36].

The optical microscope image and schematics of our silicon photonic chip are shown in Figs. 2(a) and 2(b), respectively. To obtain the multiphoton entangled state, identical photons are required. We generate frequency-degenerate photon pairs via spontaneous four wave mixing

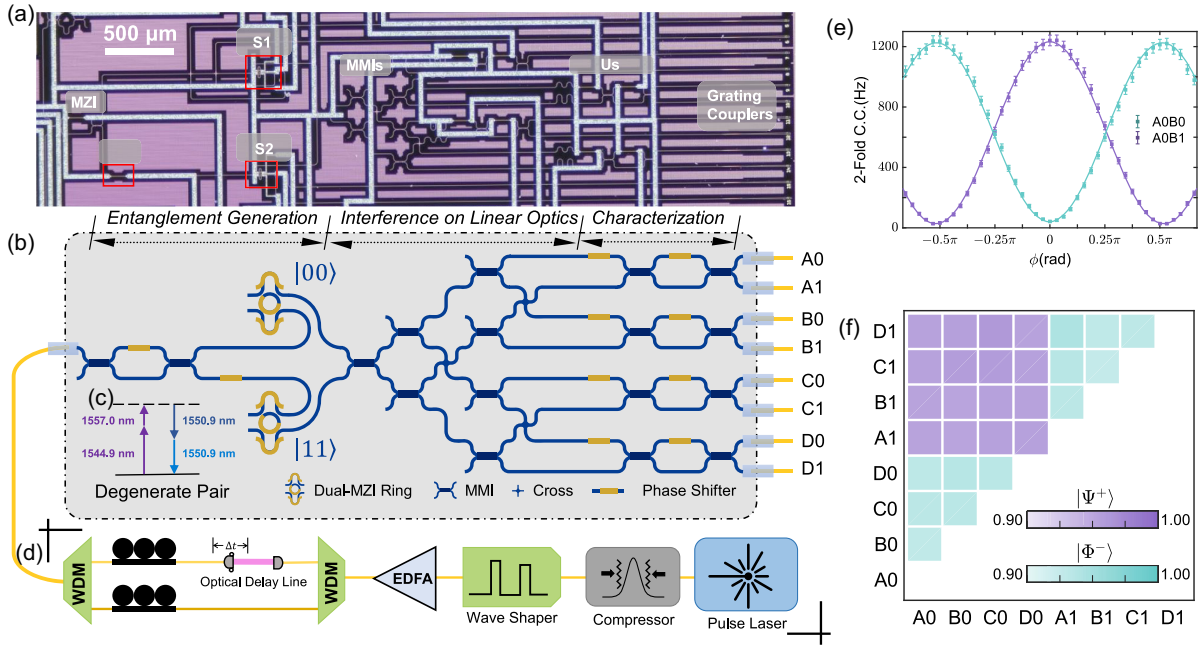

FIG. 2. Device description and experimental setup. (a) Photograph of the silicon photonic chip. Important on-chip elements are labeled: two DMZI-ring photon-pair sources (S1 and S2), multimode interference devices (MMIs), universal qubit analyzers (Us), and the phase shifter for coherent control (ϕ). (b) Experimental setup for generating and characterizing the whole family of Dicke states. Two photon pairs are created. Each pair is in a superposition between two coherently pumped DMZI-ring sources (S1 and S2), and routed by a linear optical network of MMIs to four Us, which are composed of 8 MMIs and 8 phase shifters (PSs). All photons are then coupled out from the chip, filtered, and detected by 8 grating couplers, filters, and superconducting nanowire single-photon detectors (not shown). All on-chip PSs are controlled with current sources. (c) Two different pump photons (1557.0 nm and 1544.9 nm) generate two identical photons (1550.9 nm) via nondegenerate SFWM process. (d) Dual-color pulse pumping setup to generate degenerate photon pair. A picosecond pump pulse is compressed to increase the bandwidth to over 20 nm, then selected by a wave shaper and amplified by an erbium-doped fiber amplifier (EDFA). After synchronized by WDMs and a tunable optical delay line, two color pulses are coupled into the chip. (e) Twofold coincidence counts between detectors A0 and B1 (corresponding to the projection onto $|\Psi^+\rangle$, visibility $= 95.67\% \pm 0.26\%$, purple) and A0 and B0 (corresponding to the projection onto $|\Phi^-\rangle$, visibility $= 93.42\% \pm 0.32\%$, green) show the high-quality coherent control of two-photon states, $|\Psi_2(\phi)\rangle$. (f) All 28 possible two-photon interference visibilities show the high quality and high homogeneity of our work. The average measured visibilities are $95.87\% \pm 0.07\%$ for $|\Psi^+\rangle$ (purple) and $93.76\% \pm 0.09\%$ for $|\Phi^-\rangle$ (green). Uncertainties are derived from Poissonian statistics and error propagation.

(SFWM) [Fig. 2(c)] by using a dual-color pulsed pump system [Fig. 2(d)] [49,50]. A pump laser generates picosecond pulses, whose pulse width is further broadened by a compressor to over 20 nm. Subsequently, a wave shaper filters the incoming broadband pump and select the dual-color pump pulses (1557.0 nm and 1544.9 nm, 40 GHz bandwidth each), which are further amplified by an erbium-doped fiber amplifier (EDFA). A wavelength-division-multiplexing (WDM) network enables us to control the two wavelength pulses independently. In this part, frequency noise suppression, polarization control, and time synchronization are accomplished by WDMs, polarization controllers (PCs), and an optical delay line (ODL), respectively. See Supplemental Material [36] for details on pump control.

On the silicon chip, we use two DMZI-rings [29–32] as the efficient photon-pair sources. Using these DMZI-rings, we achieve critically coupling for pump light and over-coupling for signal and idler photons at the same time. By doing so, we enhance the use of pump and achieve a high extraction rate of generated photons (see more experimental details in Supplemental Material [36]). Considering the second-order SFWM process, in which two pairs of photons (four photons) are generated at the same time, we cannot distinguish where these two pairs are generated. They can either be generated from one DMZI-ring or one pair from each DMZI-ring. The two photon pairs are then routed into a linear optical network consisted of seven cascade multimode interference devices (MMIs), acting as balanced beam splitters. At the first MMI, the photon pairs interfere via RHOM [25,33,34]. Then the remaining MMIs further separate them into four out ports: A, B, C, and D. Each port has two logic outcomes. For instance, outputs A0 and A1 in Fig. 2(b) correspond to the projection of photons into $|0\rangle_A$ and $|1\rangle_A$, respectively. At the characterization stage, each qubit is analyzed using a universal qubit analyzer, which is composed of a phase shifter (PS) and a tunable MZI. Then all photons are coupled out from the chip, filtered by off-chip WDMs,

and detected with superconducting nanowire single-photon detectors.

Results.—First, we verify the indistinguishability of two DMZI-ring photon-pair sources via RHOM interference [25,33,34], which is the prerequisite for high-quality multi-photon-state generation. Each two-photon output offers a RHOM interference fringe when scanning the relative phase ϕ. The coincidence counts with the same path mode (such as A0 and B0) correspond to photon pair in $|\Phi^-\rangle$ [green curve in Fig. 2(e)]; the coincidence counts with different path modes (such as A0 and B1) show the complemented results, corresponding to the photon pair in $|\Psi^+\rangle$ [purple curve in Fig. 2(e)]. We have thoroughly investigated all 28 possible curves and show their visibility results in Fig. 2(f). The average measured visibilities are $95.87\% \pm 0.07\%$ for $|\Psi^+\rangle$ state and $93.76\% \pm 0.07\%$ for $|\Phi^-\rangle$ state. These high visibility fringes indicate the high quality of spectral overlap and qubit entanglement. The deviation of visibilities is mainly due to multiphoton generation events. The higher accidental coincidence from the frequency-degenerate photons may account for the lower visibility of $|\Phi^-\rangle$ state (see analysis in the Supplemental Material [36]).

Having established a high-quality two-photon qubit source, we next investigate the four-photon state when there are two pairs of photons generated in the same pulse. The estimated pair-generation rate is ~0.003 per pulse with ~1.3 mW pulse pump laser coupled onto the chip (a factor of about 500 less than those used in bulk optical experiment [10]). To verify the state quality, we choose two special cases of $|\Psi(\phi)\rangle$ and characterize them via complete quantum state tomography [51]: setting $\phi = 0$ results in a symmetric Dicke state $|\Psi(0)\rangle = |D_4^2\rangle$; setting $\phi = \pi/2$ results in a four-photon state with the superposition of GHZ state and symmetric Dicke state: $|\Psi(\pi/2)\rangle = 1/2\sqrt{6}(-3|0000\rangle + |0011\rangle + |0101\rangle + |0110\rangle + |1001\rangle + |1010\rangle + |1100\rangle - 3|1111\rangle)$. We use 81 settings of all possible combinations of three Pauli bases applied on each photon: $\{|0\rangle, |1\rangle\}$,$\{|+\rangle, |-\rangle\}$, and $\{|L\rangle, |R\rangle\}$, where $|+/-\rangle = 1/\sqrt{2}(|0\rangle \pm |1\rangle)$ and $|L/R\rangle = 1/\sqrt{2}(|0\rangle \pm i|1\rangle)$. The tomography measurement takes approximately 3 h per setting and we obtain a total fourfold count of about 1000 for each setting. Figure 3 displays the real part of measured and ideal density matrices for $|\Psi(0)\rangle$ and $|\Psi(\pi/2)\rangle$, respectively. The imaginary part is negligibly small. From experimentally obtained density matrices (ρ_{exp}), we estimate the four-photon state quality with state fidelity to the ideal state (ρ_{ideal}) and obtain the fidelities of 0.817 ± 0.003 for $|\Psi(0)\rangle$ and 0.829 ± 0.003 for $|\Psi(\pi/2)\rangle$, respectively. Here, the fidelity is defined as $F = \text{Tr}(\rho_{\text{exp}}\rho_{\text{ideal}})$, and the uncertainty is obtained from Monte Carlo simulation with Poisson statistics. These results show the high quality of our multiphoton source maintains when changing the relative phase ϕ, indicating that various multiphoton entangled states can be generated

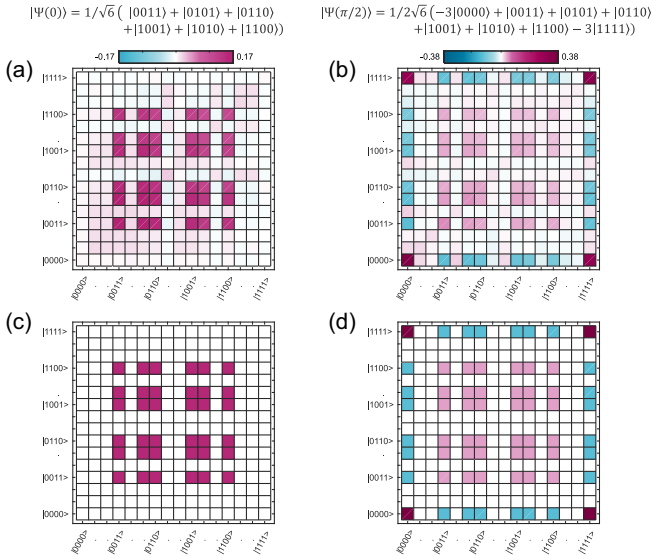

FIG. 3. Real part of the density matrix for different states. (a) The symmetric Dicke state $|D_4^2\rangle$ by setting $\phi = 0$. (b) The superposition of four-photon GHZ state $|GHZ_4\rangle$ and symmetric Dicke state $|D_4^2\rangle$ by setting $\phi = \pi/2$. The experimentally obtained quantum-state fidelities are 0.817 ± 0.003 for $|\Psi(0)\rangle$ and 0.829 ± 0.003 for $|\Psi(\pi/2)\rangle$, respectively. The ideal density matrix for $|\Psi(0)\rangle$ and $|\Psi(\pi/2)\rangle$ are shown in (c) and (d), respectively. Uncertainties are obtained from 100 Monte Carlo simulations with counting Poisson statistics.

on one chip with coherent control. For the symmetric Dicke state, $|D_4^2\rangle$, we perform the single-qubit projective measurements in different bases and show the conversion between GHZ and W states. We also measure the singlet fraction of the state, showing high robustness against loss of photons and its potential in quantum networking. See Supplemental Material [36] for details.

Unlike the two-photon Bell State where the relative phase ϕ can change $|\Psi^+>$ to $|\Phi^->$, it is nontrivial to see what happens to the four photons and how the phase ϕ controls all four photons. First, let us rewrite Eq. (3) into the mutually unbiased basis of $\{|L\rangle, |R\rangle\}$:

$$|\Psi_4(\phi)\rangle = \frac{1}{2\sqrt{6}}(-3e^{-2i\phi}|LLLL\rangle + |LLRR\rangle + |LRLR\rangle + |LRRL\rangle + |RLLR\rangle + |RLRL\rangle + |RRLL\rangle - 3e^{2i\phi}|RRRR\rangle), \quad (4)$$

which can be viewed as a superposition of a GHZ state and a symmetric Dicke state. One can see that in this basis, the collective phase ϕ has no influence on the amplitude of each term. Therefore, when we tune ϕ and measure four photons in $\{|L\rangle, |R\rangle\}$ basis, the probabilities of fourfold coincidence stay the same. The theoretical results and the experimental results are shown in Figs. 4(a) and 4(b), respectively, which agree well with each other. In order to prove the coherence of our collective control, we further measure four photons in the $\{|0\rangle, |1\rangle\}$ basis and observe

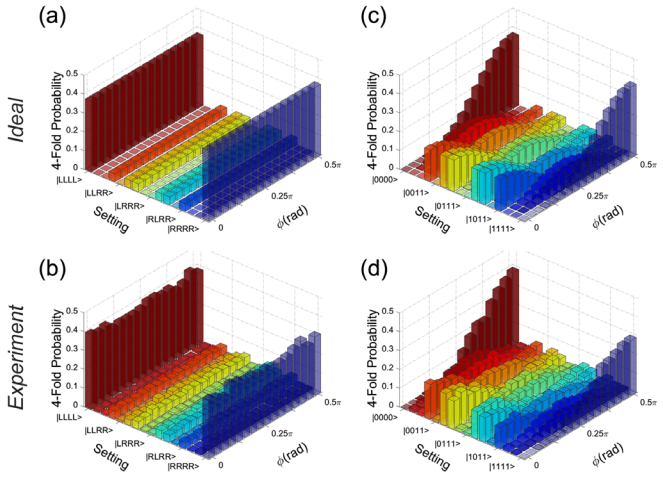

FIG. 4. Collectively coherent control of the four-photon state. (a),(b) The expected ideal and experimentally measured coincidence distributions for photons measured in the mutually unbiased basis of $\{|L\rangle, |R\rangle\}$. The distributions remain constant independently of the relative phase ϕ. (c),(d) The ideal and experimental cases for photons measured in the computational basis of $\{|0\rangle, |1\rangle\}$. The relative pump phase ϕ rotates the whole family of Dicke state coherently.

that each of the fourfold coincidences coherently varies with phase ϕ. We show the theoretical calculations and the experimental results in Figs. 4(c) and 4(d), respectively. To show the agreement between theory and experiment, we calculate the overlap of experimental distribution changes with theoretical cases via the similarity $S = (\int \sqrt{\Gamma_{\text{exp}}\Gamma_{\text{ideal}}})^2/(\int \Gamma_{\text{exp}} \int \Gamma_{\text{ideal}})$, where Γ_{exp} (Γ_{ideal}) is the experimental (ideal) fourfold coincidence distribution changing with phase ϕ. We obtain the similarity 0.9209 ± 0.0015 for $\{|L\rangle, |R\rangle\}$ basis and 0.9655 ± 0.0012 for $\{|H\rangle, |V\rangle\}$ basis, respectively. The experimental results fit well with the expectation, showing the evolution of the whole family of Dicke states. One can further rewrite Eq. (4) into the rotated basis $\{|\theta\rangle, |\theta_\perp\rangle\} = \{\binom{\sin\phi/2}{\cos\phi/2}, \binom{\cos\phi/2}{-\sin\phi/2}\}$ and obtain the symmetric four-photon Dicke state in such basis [36].

Conclusions.—We have presented a single monolithic silicon chip capable of observing the superposition of all five Dicke states with high fidelity by employing resonance-enhanced photon-pair sources. With this device, we have demonstrated the on-chip collectively coherent control of both the two-photon Bell states and the four-photon Dicke states. The experimental setup and methods are generic for observation and coherent control of the entire family of Dicke states with more photon numbers. Such a large-scale integrated quantum circuit can offer the opportunity to generate multiphoton states with larger Hilbert spaces. Although the efficiency to observe states would inevitably decrease with the photon numbers, studying these multiphoton states is important to explore the key techniques of quantum networking, quantum computing, and quantum communication. Our study extends the range of attainable multipartite quantum states in silicon, which has potential for applications in multiparty quantum networking and quantum enhanced metrology.

This research was supported by the National Key Research and Development Program of China (Grants No. 2022YFE0137000, No. 2019YFA0308704, and No. 2017YFA0303704), the National Natural Science Foundation of China (Grants No. 11690032 and No. 11321063), the NSFC-BRICS (Grant No. 61961146001), the Leading-Edge Technology Program of Jiangsu Natural Science Foundation (Grant No. BK20192001), the Fundamental Research Funds for the Central Universities, the Innovation Program for Quantum Science and Technology (Grant No. 2021ZD0301500).

*Corresponding author.
xiaosong.Ma@nju.edu.cn

[1] R. Horodecki, P. Horodecki, M. Horodecki, and K. Horodecki, Quantum entanglement, Rev. Mod. Phys. **81**, 865 (2009).
[2] R. Raussendorf and H. J. Briegel, A One-Way Quantum Computer, Phys. Rev. Lett. **86**, 5188 (2001).
[3] P. Walther, K. J. Resch, T. Rudolph, E. Schenck, H. Weinfurter, V. Vedral, M. Aspelmeyer, and A. Zeilinger, Experimental one-way quantum computing, Nature (London) **434**, 169 (2005).
[4] D. E. Browne and T. Rudolph, Resource-Efficient Linear Optical Quantum Computation, Phys. Rev. Lett. **95**, 010501 (2005).
[5] R. Raussendorf, J. Harrington, and K. Goyal, Topological fault-tolerance in cluster state quantum computation, New J. Phys. **9**, 199 (2007).
[6] D. Leibfried, M. D. Barrett, T. Schaetz, J. Britton, J. Chiaverini, W. M. Itano, J. D. Jost, C. Langer, and D. J. Wineland, Toward Heisenberg-limited spectroscopy with multiparticle entangled states, Science **304**, 1476 (2004).
[7] L. Pezzé and A. Smerzi, Entanglement, Nonlinear Dynamics, and the Heisenberg Limit, Phys. Rev. Lett. **102**, 100401 (2009).
[8] L.-Z. Liu, Y.-Z. Zhang, Z.-D. Li, R. Zhang, X.-F. Yin, Y.-Y. Fei, L. Li, N.-L. Liu, F. Xu, Y.-A. Chen *et al.*, Distributed quantum phase estimation with entangled photons, Nat. Photonics **15**, 137 (2021).
[9] R. H. Dicke, Coherence in spontaneous radiation processes, Phys. Rev. **93**, 99 (1954).
[10] N. Kiesel, C. Schmid, G. Tóth, E. Solano, and H. Weinfurter, Experimental Observation of Four-Photon Entangled Dicke State with High Fidelity, Phys. Rev. Lett. **98**, 063604 (2007).
[11] R. Prevedel, G. Cronenberg, M. S. Tame, M. Paternostro, P. Walther, M.-S. Kim, and A. Zeilinger, Experimental Realization of Dicke States of up to Six Qubits for Multiparty Quantum Networking, Phys. Rev. Lett. **103**, 020503 (2009).
[12] R. Krischek, C. Schwemmer, W. Wieczorek, H. Weinfurter, P. Hyllus, L. Pezzé, and A. Smerzi, Useful Multiparticle Entanglement and Sub-Shot-Noise Sensitivity in Experimental Phase Estimation, Phys. Rev. Lett. **107**, 080504 (2011).

[13] R. Ionicioiu, A. E. Popescu, W. J. Munro, and T. P. Spiller, Generalized parity measurements, Phys. Rev. A **78**, 052326 (2008).
[14] W. Wieczorek, R. Krischek, N. Kiesel, P. Michelberger, G. Tóth, and H. Weinfurter, Experimental Entanglement of a Six-Photon Symmetric Dicke State, Phys. Rev. Lett. **103**, 020504 (2009).
[15] H. Häffner, W. Hänsel, C. Roos, J. Benhelm, D. Chek-al Kar, M. Chwalla, T. Körber, U. Rapol, M. Riebe, P. Schmidt *et al.*, Scalable multiparticle entanglement of trapped ions, Nature (London) **438**, 643 (2005).
[16] F. Haas, J. Volz, R. Gehr, J. Reichel, and J. Estève, Entangled states of more than 40 atoms in an optical fiber cavity, Science **344**, 180 (2014).
[17] R. McConnell, H. Zhang, J. Hu, S. Ćuk, and V. Vuletić, Entanglement with negative Wigner function of almost 3,000 atoms heralded by one photon, Nature (London) **519**, 439 (2015).
[18] Y.-Q. Zou, L.-N. Wu, Q. Liu, X.-Y. Luo, S.-F. Guo, J.-H. Cao, M. K. Tey, and L. You, Beating the classical precision limit with spin-1 Dicke states of more than 10,000 atoms, Proc. Natl. Acad. Sci. U.S.A. **115**, 6381 (2018).
[19] E. Lucero, R. Barends, Y. Chen, J. Kelly, M. Mariantoni, A. Megrant, P. O'Malley, D. Sank, A. Vainsencher, J. Wenner *et al.*, Computing prime factors with a Josephson phase qubit quantum processor, Nat. Phys. **8**, 719 (2012).
[20] J. A. Mlynek, A. A. Abdumalikov, J. M. Fink, L. Steffen, M. Baur, C. Lang, A. F. van Loo, and A. Wallraff, Demonstrating *W*-type entanglement of Dicke states in resonant cavity quantum electrodynamics, Phys. Rev. A **86**, 053838 (2012).
[21] Z. Wang, H. Li, W. Feng, X. Song, C. Song, W. Liu, Q. Guo, X. Zhang, H. Dong, D. Zheng *et al.*, Controllable Switching Between Superradiant and Subradiant States in a 10-Qubit Superconducting Circuit, Phys. Rev. Lett. **124**, 013601 (2020).
[22] X. Cao, M. Zopf, and F. Ding, Telecom wavelength single photon sources, J. Semicond. **40**, 071901 (2019).
[23] J. Wang, F. Sciarrino, A. Laing, and M. G. Thompson, Integrated photonic quantum technologies, Nat. Photonics **14**, 273 (2020).
[24] E. Pelucchi, G. Fagas, I. Aharonovich, D. Englund, E. Figueroa, Q. Gong, H. Hannes, J. Liu, C.-Y. Lu, N. Matsuda *et al.*, The potential and global outlook of integrated photonics for quantum technologies, Nat. Rev. Phys. **4**, 194 (2022).
[25] J. W. Silverstone, R. Santagati, D. Bonneau, M. J. Strain, M. Sorel, J. L. O'Brien, and M. G. Thompson, Qubit entanglement between ring-resonator photon-pair sources on a silicon chip, Nat. Commun. **6**, 7948 (2015).
[26] S. Paesani, M. Borghi, S. Signorini, A. Maïnos, L. Pavesi, and A. Laing, Near-ideal spontaneous photon sources in silicon quantum photonics, Nat. Commun. **11**, 2505 (2020).
[27] D. Llewellyn, Y. Ding, I. I. Faruque, S. Paesani, D. Bacco, R. Santagati, Y.-J. Qian, Y. Li, Y.-F. Xiao, M. Huber *et al.*, Chip-to-chip quantum teleportation and multi-photon entanglement in silicon, Nat. Phys. **16**, 148 (2020).
[28] J. C. Adcock, C. Vigliar, R. Santagati, J. W. Silverstone, and M. G. Thompson, Programmable four-photon graph states on a silicon chip, Nat. Commun. **10**, 3528 (2019).
[29] C. Tison, J. Steidle, M. Fanto, Z. Wang, N. Mogent, A. Rizzo, S. Preble, and P. Alsing, Path to increasing the coincidence efficiency of integrated resonant photon sources, Opt. Express **25**, 33088 (2017).
[30] Z. Vernon, M. Menotti, C. Tison, J. Steidle, M. Fanto, P. Thomas, S. Preble, A. Smith, P. Alsing, M. Liscidini *et al.*, Truly unentangled photon pairs without spectral filtering, Opt. Lett. **42**, 3638 (2017).
[31] L. Lu, L. Xia, Z. Chen, L. Chen, T. Yu, T. Tao, W. Ma, Y. Pan, X. Cai, Y. Lu *et al.*, Three-dimensional entanglement on a silicon chip, npj Quantum Inf. **6**, 30 (2020).
[32] Y. Liu, C. Wu, X. Gu, Y. Kong, X. Yu, R. Ge, X. Cai, X. Qiang, J. Wu, X. Yang *et al.*, High-spectral-purity photon generation from a dual-interferometer-coupled silicon microring, Opt. Lett. **45**, 73 (2020).
[33] J. Chen, K. F. Lee, and P. Kumar, Deterministic quantum splitter based on time-reversed Hong-Ou-Mandel interference, Phys. Rev. A **76**, 031804(R) (2007).
[34] J. W. Silverstone, D. Bonneau, K. Ohira, N. Suzuki, H. Yoshida, N. Iizuka, M. Ezaki, C. M. Natarajan, M. G. Tanner, R. H. Hadfield *et al.*, On-chip quantum interference between silicon photon-pair sources, Nat. Photonics **8**, 104 (2014).
[35] M. Eibl, N. Kiesel, M. Bourennane, C. Kurtsiefer, and H. Weinfurter, Experimental Realization of a Three-Qubit Entangled W State, Phys. Rev. Lett. **92**, 077901 (2004).
[36] See Supplemental Material at http://link.aps.org/supplemental/10.1103/PhysRevLett.130.223601 for theoretical and experimental details, which includes Refs. [10,11,29–32,37–48].
[37] P. Zhu, S. Xue, Q. Zheng, C. Wu, X. Yu, Y. Wang, Y. Liu, X. Qiang, M. Deng, J. Wu *et al.*, Reconfigurable multiphoton entangled states based on quantum photonic chips, Opt. Express **28**, 26792 (2020).
[38] M. Krenn, X. Gu, and A. Zeilinger, Quantum Experiments and Graphs: Multiparty States as Coherent Superpositions of Perfect Matchings, Phys. Rev. Lett. **119**, 240403 (2017).
[39] X. Gu, M. Erhard, A. Zeilinger, and M. Krenn, Quantum experiments and graphs II: Quantum interference, computation, and state generation, Proc. Natl. Acad. Sci. U.S.A. **116**, 4147 (2019).
[40] X. Gu, L. Chen, A. Zeilinger, and M. Krenn, Quantum experiments and graphs. III. High-dimensional and multiparticle entanglement, Phys. Rev. A **99**, 032338 (2019).
[41] Z. Y. Ou and Y. J. Lu, Cavity Enhanced Spontaneous Parametric Down-Conversion for the Prolongation of Correlation Time Between Conjugate Photons, Phys. Rev. Lett. **83**, 2556 (1999).
[42] D. Klyshko, Use of two-photon light for absolute calibration of photoelectric detectors, Sov. J. Quantum Electron. **10**, 1112 (1980).
[43] A. Christ, K. Laiho, A. Eckstein, K. N. Cassemiro, and C. Silberhorn, Probing multimode squeezing with correlation functions, New J. Phys. **13**, 033027 (2011).
[44] R. Grobe, K. Rzazewski, and J. Eberly, Measure of electron-electron correlation in atomic physics, J. Phys. B **27**, L503 (1994).
[45] A. Sen(De), U. Sen, M. Wieśniak, D. Kaszlikowski, and M. Żukowski, Multiqubit *W* states lead to stronger nonclassicality than Greenberger-Horne-Zeilinger states, Phys. Rev. A **68**, 062306 (2003).

[46] M. Murao, D. Jonathan, M. B. Plenio, and V. Vedral, Quantum telecloning and multiparticle entanglement, Phys. Rev. A **59**, 156 (1999).

[47] M. Horodecki, P. Horodecki, and R. Horodecki, General teleportation channel, singlet fraction, and quasidistillation, Phys. Rev. A **60**, 1888 (1999).

[48] N. Gisin and S. Massar, Optimal Quantum Cloning Machines, Phys. Rev. Lett. **79**, 2153 (1997).

[49] S. Paesani, Y. Ding, R. Santagati, L. Chakhmakhchyan, C. Vigliar, K. Rottwitt, L. K. Oxenløwe, J. Wang, M. G. Thompson, and A. Laing, Generation and sampling of quantum states of light in a silicon chip, Nat. Phys. **15**, 925 (2019).

[50] L.-T. Feng, M. Zhang, Z.-Y. Zhou, Y. Chen, M. Li, D.-X. Dai, H.-L. Ren, G.-P. Guo, G.-C. Guo, M. Tame *et al.*, Generation of a frequency-degenerate four-photon entangled state using a silicon nanowire, npj Quantum Inf. **5**, 90 (2019).

[51] D. F. V. James, P. G. Kwiat, W. J. Munro, and A. G. White, Measurement of qubits, Phys. Rev. A **64**, 052312 (2001).